

DEVELOPMENT OF DENSITY-GRADED SANDWICH STRUCTURES WITH IN-SITU FOAMING FILAMENTS IN ADDITIVE MANUFACTURING

Márton Tomin¹, Norbert Lukács¹, Szabolcs Berezvai²

¹Department of Polymer Engineering, Budapest University of Technology and Economics

²Department of Applied Mechanics, Budapest University of Technology and Economics

Abstract

This study investigates using in-situ foamable filaments in extrusion-based additive manufacturing to create density-graded sandwich structures. By varying printing temperatures, we analyzed the foam density, cell structure, and mechanical properties. We also outlined a finite strain viscoelastic-viscoplastic material model for future optimization of layer configuration. The findings highlight the importance of printing temperature adjustment in achieving uniform cell structures and enhanced mechanical properties.

Introduction

Advances in extrusion-based additive manufacturing technologies have enabled the cost-effective production of complex geometries, customized and small series products [1]. In parallel with technological innovation, the use of compostable biopolymers from renewable sources is becoming more and more important due to stricter environmental directives and increased focus on sustainability [2, 3].

There is also a growing focus on developments to reduce the weight of products, not only to reduce CO₂ emissions during transportation, but foams also provide better insulation and shock absorption properties compared to solid materials due to their porous structure [4-6].

Our previous research [7] has demonstrated that multilayer foam structures with different densities in each layer can be used to increase the shock-absorbing capacity of products. However, these sandwich structures can currently only be produced in two technological steps, so the use of in-situ foaming filaments in 3D printing could bring a breakthrough in the production of sandwich structures [8, 9].

In-situ foaming involves the use of expandable filaments, where foam expansion occurs during the 3D printing process. This method allows the creation of functionally graded foams with controlled porosity and graded density structures, enhancing energy absorption and efficient material use [10].

Several approaches have been explored to achieve cellular structures in thermoplastics during the material extrusion additive manufacturing process, such as the incorporation of the filament with CO₂ gas [11], the use of chemical blowing agents [12, 13], and the incorporation of thermally expandable microspheres (TEMs) in the filament [14, 15]. These techniques offer advantages such as low material usage, ease of microstructure control, and mitigation of shrinkage and inter-bead voids in 3D-printed parts. By controlling the printing parameters, it is also possible to create structures with a continuously varying density gradient, which not only optimizes mechanical properties but also reduces production time and costs [10].

The aim of our research was to create density-graded sandwich structures using biopolymer-based in-situ foaming filaments and to analyze the effect of the layer order variation on the flexural mechanical properties. Firstly, we investigated the effect of printing temperature on foam density, cell structure, and mechanical strength using in-situ foaming filament. Then, we aimed to perform preliminary tests in order to develop a visco-hyperelastic material model, which can be used in the future to determine the optimum layer order for a given load by finite element simulation. Recent studies have analyzed the change in the finite strain behavior of 3D-printed foams, including using the phenomenological hyperelastic modeling approach [16-18]. In the proposed models, the hyperelastic material parameters are determined as a function of various technological parameters, thus providing an easy-to-implement constitutive model for the finite element analysis of such structures. Finally, multilayer structures were fabricated by varying the printing parameters during production in a targeted way, and the effect of the change in the layer order on the flexural strength was investigated.

Materials

The test specimens were printed using a commercially available, 1.75 mm diameter filament (LW-PLA manufactured by COLORFABB B.V. (Belfeld, The Netherlands)), which has a different expansion rate during production depending on the printing temperature. The polylactic acid (PLA) material used as the filament base

material has a glass transition temperature range of 55-60°C, a melting temperature of 150-160°C, and a melt flow index of 6 g/10 min (210°C/2.16 kg). The decomposition temperature of the foaming agent is ±230°C according to the manufacturer’s data sheet, and the heat deflection temperature (HDT-B, ISO 75) of the material is 60°C.

Methods

Extrusion-based additive manufacturing

The production of the specimens using FDM technology was performed on an “Original Prusa Mini” (Prusa Research, Prague, Czech Republic) printer with a useful working area of 180x180x180 mm. In addition, an E3D V6 plated copper nozzle with a diameter of 0.4 mm was used. For the printing of the test specimens, the default “Original Prusa MINI+” and “0.20 mm QUALITY” settings were chosen. The printing parameters were 0.2 mm layer height, 100% infill, and a “rectilinear” fill pattern with a fill angle of ±45°. The print speed was set to 140 mm/s for the infill and 50 mm/s for the perimeters.

During the preliminary tests, we found that the filament starts to foam above 190°C and the manufacturer’s data sheet recommends processing up to 250°C, so we set the nozzle temperature to between 190-250°C depending on the specimen, and the bed temperature to 60°C. Accordingly, specimens for density measurement, microscopy, and tensile testing were prepared at seven different temperatures ranging from 190°C to 250°C with 10°C step intervals to investigate the effect of printing temperature.

In addition, for flexural testing, we produced sandwich structures with varying densities per layer with the printing temperatures set at 190/230/230/190°C and 190/200/210/230°C per layer (see Figure 1). The mechanical test results were evaluated for these samples by comparing them with the results of the single-density sample (printed at constant 200°C), which had the same density as the average density of the multilayer samples.

TYPE A	TYPE B
T=190°C	T=230°C
T=200°C	T=210°C
T=210°C	T=200°C
T=230°C	T=190°C
TYPE C	reference
T=190°C	T=200°C
T=230°C	T=200°C
T=230°C	T=200°C
T=190°C	T=200°C

Figure 1. Printing temperature during the production of the multilayer, density-graded foam structures

Density measurement

To determine the degree of foaming of the filament at different temperatures, hollow cubes of 20x20x20 mm (open at the top) were printed. These cubes had the same wall thickness in the 3D model, but in reality, they differed because the foaming at different production temperatures caused their volumes to expand differently (Figure 2).

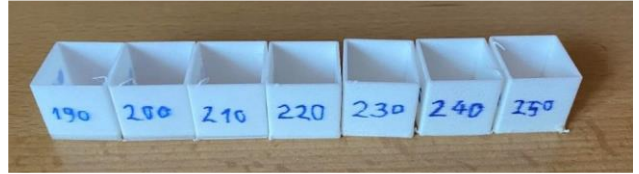


Figure 2. Test specimens produced to investigate the effect of printing temperature on foaming

After determining the wall thicknesses, the change in volume due to foaming was compensated by adjusting the extrusion ratio applied during printing, which is proportional to the relative density:

$$e = \frac{w_0}{w_i} \quad (1)$$

where e (-) is the extrusion ratio, w_0 (mm) is the wall thickness of the calibration cube printed with an unfoamed filament, and w_i (mm) is the wall thickness of the calibration cube printed with a foamed filament.

Scanning electron microscopy

The cell structure of the samples produced at different printing temperatures was investigated using a JEOL JSM 6380LA scanning electron microscope (Jeol, Tokyo, Germany). The samples were prepared by immersing them in liquid nitrogen prior to testing to create cryogenic fracture surfaces, and then coated with gold-palladium alloy to ensure proper conductivity. From the electron microscopic images and the density of the samples, we determined their relative density (2), the degree of expansion (3), and from these the cell density (4) and the average cell wall thickness (5) [19].

$$\rho_{rel} = \frac{\rho_{foam}}{\rho_{solid}} [-] \quad (2)$$

$$\phi = \frac{1}{\rho_{rel}} [-] \quad (3)$$

$$N_C = \left(\frac{n}{A}\right)^{\frac{3}{2}} \left[\frac{pcs}{cm^3}\right] \quad (4)$$

$$\delta = \left(\sqrt[3]{\frac{\phi}{\phi - 1}} - 1 \right) \cdot l [\mu m] \quad (5)$$

where ρ_{rel} is the relative density (-), ρ_{foam} is the foam density (kg/m^3), ρ_{solid} is the density of the unfoamed filament (kg/m^3), ϕ is the degree of expansion (-), N_c is the cell density (pcs/cm^3), n is the number of cells visible in the SEM image (pcs), A is the investigated area on the sample (cm^2), δ is the cell wall thickness (μm), and l is the average cell size (μm). The average cell size was determined by image processing. All parameters were determined from SEM images taken from the middle of specimens where the print speed was set to 140 mm/sec.

Mechanical characterization

Tensile tests

Uniaxial tensile tests were carried out on a Zwick Z005 universal testing machine (Zwick, Ulm, Germany). During the tensile test, the crosshead displacement speed was 5 mm/min, and the preload was 10 N. The tensile test specimens were produced following the DIN EN ISO 527-2 type 1B standard, with enclosure dimensions of 150x10x4 mm. The initial spacing between the grips was set to 115 mm. The loads were recorded using a 5 kN load capacity cell. From the measured force-displacement values, the engineering stress and the engineering strain were computed. To evaluate the effect of printing temperature, the relative tensile strength was determined, which can be calculated as the quotient of the stress recorded at the peak force and the relative density (which is equal to the extrusion ratio):

$$\sigma_{rel} = \frac{\sigma_m}{e} \quad (6)$$

where σ_{rel} is the relative tensile strength (MPa), and σ_m is the tensile strength calculated from the peak force (MPa).

Since the matrix material is thermoplastic, the mechanical characterization also aimed to reveal the viscoelastic-viscoplastic properties and their changes with the foam density. For this, a preliminary uniaxial cyclic tensile test was also performed, which consists of several loading-unloading cycles with increasing displacements (see Figure 3). The cyclic loading test consisted of five displacement-controlled uploading phases with a constant strain rate of $\dot{\epsilon} = 0.001$ 1/s. The prescribed strain levels were $\epsilon = 0.022, 0.045, 0.068, 0.091,$ and 0.113 , respectively. Each uploading phase was then followed by a holding phase for $t_{rel} = 600$ s. After that a force controlled unloading phase was inserted back to 0.5 N with unload speed of $v_{unload} = 0.5$ N/s. Finally, after the unloading phase, a holding phase was applied for $t_{rel} = 600$ s again.

During the tensile tests, the displacements were also recorded using a Mercury Monet (Sobriety, Kurim, Czech Republic) optical strain measuring system (DIC).

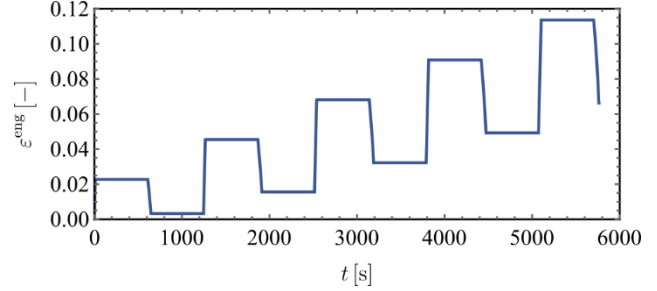


Figure 3. Loading history applied during the uniaxial cyclic tensile tests

Flexural tests

In the flexural test, we aimed to investigate the effect of changing the layer order by testing the multilayer structures illustrated in Figure 1. The tests were performed on a Zwick Z005 machine with a 5-mm/min test speed and 1 N preload. The bending specimens produced were in accordance with the ISO/R 178 standard, having an enclosure dimension of 80x10x4 mm. The support distance was set 64 mm. The results were evaluated by determining the flexural strength at a deflection corresponding to 10% of the support spacing (7):

$$\sigma_{bh} = \frac{3Fl}{2bh^2} \quad (7)$$

where σ_{bh} is the flexural strength (MPa), F is the force recorded at 10% bending (N), L is the support distance (mm), b is the specimen width (mm), while h is the specimen height (mm).

Results

Density measurement

The variation of the extrusion ratio used to compensate for the volume change induced by the expansion during printing as a function of temperature is shown in Figure 4.

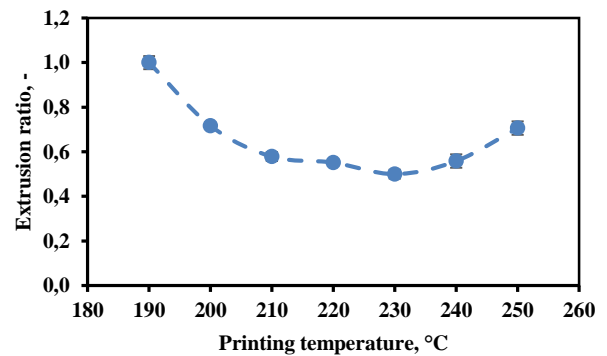


Figure 4. Expansion ratio (relative density) in the function of printing temperature

It can be observed that with the settings used, the foaming of the material starts above 190°C, and the maximum expansion occurs at 230°. However, as the printing temperature further increased, the foam density started to increase again. This tendency can be related to the decreasing viscosity with temperature. At low temperatures, high melt strength inhibits expansion, while at high temperatures, too low melt strength leads to the collapse of the evolving cells.

Scanning electron microscopy

The scanning electron microscopic images of the samples produced at different printing temperatures are shown in Figure 5.

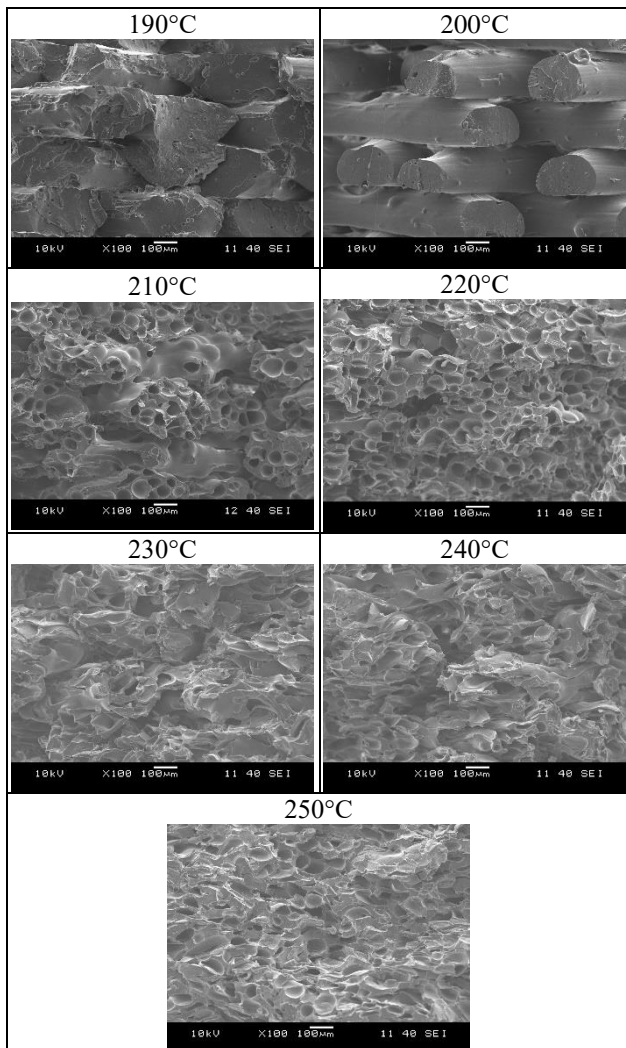


Figure 5. SEM images taken from the infill part of specimens produced at different printing temperatures

Analysis of the cell structural data (Table 1) shows that significant cell growth is first observed at 210°C, while at lower temperatures, the expansion was inhibited by too high melt strength. With increasing production temperature

from 210°C to 220°C, the average cell diameter did not change significantly, but the cell density started to increase, i.e., more cells were formed in the foam structure. It was also observed that above 230°C, due to the decrease in the melt strength, some of the cells collapsed, leading to an inhomogeneous cell structure with a lower average number of cells in a given volume (cell density).

Table 1. Cell structural properties of the specimens printed on different temperatures

Temp. (°C)	N_c (cells/cm ³)	δ (μm)	l (μm)
190	-	-	-
200	-	-	-
210	1517975	14.7	44.2 ± 15.7
220	3141877	10.0	44.0 ± 16.1
230	1501855	12.0	46.2 ± 18.1
240	1374982	14.5	46.3 ± 15.4
250	1312958	22.5	44.7 ± 16.9

Mechanical characterization

Tensile tests

The results of the uniaxial tensile tests are illustrated in Figure 6.

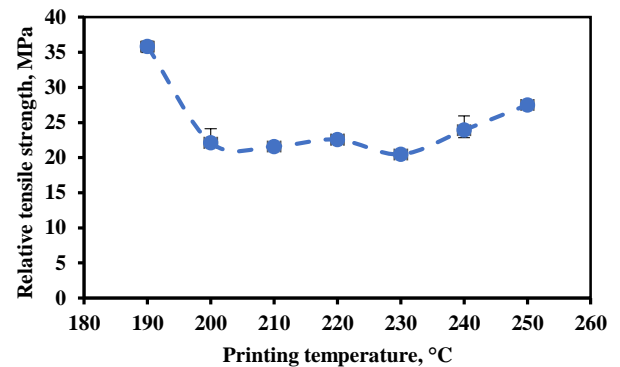


Figure 6. The relative tensile strength in the function of the printing temperature

The results show that the foaming process reduced the tensile strength of the material, but there was no significant difference between the foamed samples. Among the foamed samples, the specimen printed at 220°C showed the most favorable results in terms of strength-to-mass ratio, probably due to its more homogeneous cell structure (as seen in Figure 5).

Modelling of transverse stretch characteristics

In addition, to evaluate the effect of printing parameters, the material characterization aimed to provide a suitable finite strain material model that can characterize the elastic behavior of the mechanical behavior of 3D printed foams with different densities.

The first step of the material characterization process is to determine the transverse stretches from the change of the specimen width, namely $\lambda_T = W/W_0$. For this, image processing method was applied to the DIC images of the uniaxial tensile tests. Then, the ground Poisson's ratio was calculated using the modeling approach of the generalized Poisson's ratio [20] for finite strains using true-strains, as

$$\nu = -\varepsilon_T^{\text{true}} / \varepsilon^{\text{true}} = -\ln(\lambda_T) / \ln(\lambda) \quad (8)$$

where λ is the longitudinal stretch obtained from experiments at (a) undeformed and (b) maximally deformed states. The results show (see Figure 7) that as the printing temperature increases and simultaneously the foaming initiates, the Poisson's ratio decreases. As it is indicated in Figure 4, the maximal foaming is reached at 230 °C, therefore it can also be assumed that the Poisson's ratio also reached it minimum at this printing temperature. The calculation of the Poisson's ratio also indicates that the material shows significant volumetric deformation. The derived information of the transverse stretch properties should be directly included in the finite strain constitutive model through the generalized Poisson's ratio.

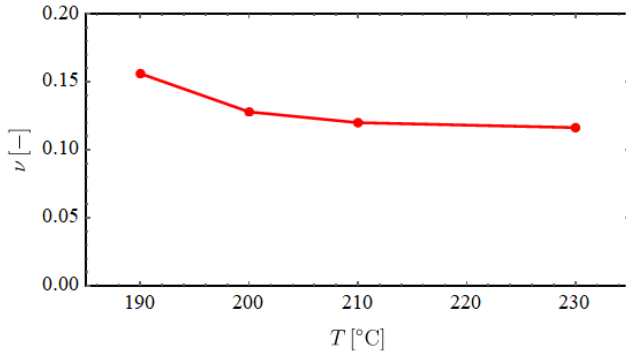


Figure 7. The variation of the Poisson's ratio with the printing temperature

The results of the cyclic tensile tests are shown in Figure 8, where the engineering stress (first Piola-Kirchhoff stress) $P = F/A_0$ and the engineering strain $\varepsilon^{\text{eng}} = u/L_0$ is shown.

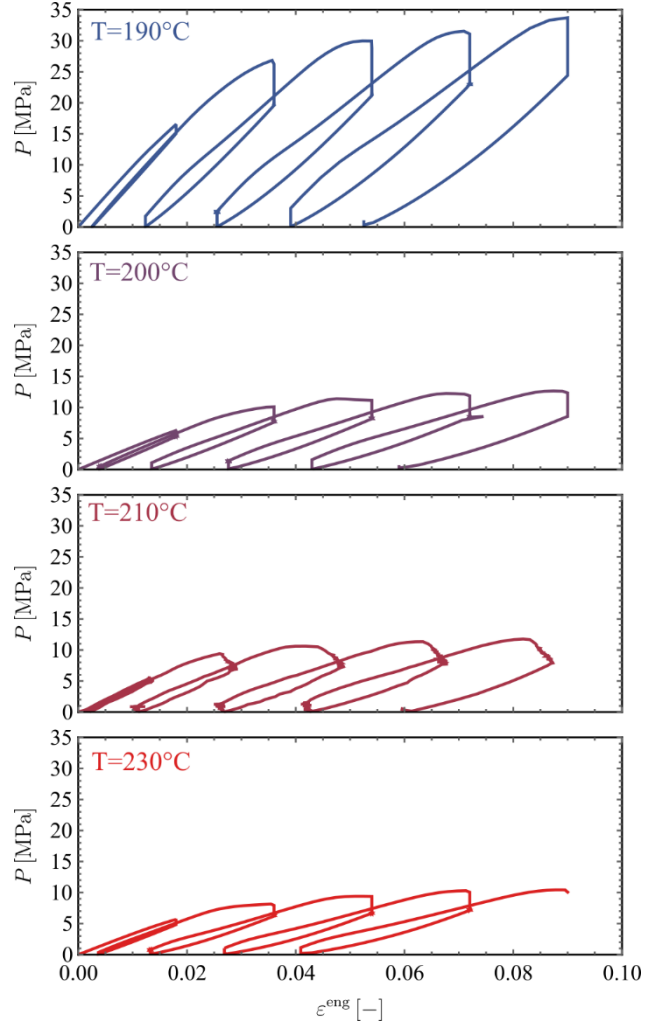


Figure 8. The viscoelastic-viscoplastic properties of the 3D printed specimens revealed by the cyclic uniaxial tensile tests for specimens printed at 190, 200, 210, and 230 °C

It is visible that at all printing temperatures, the thermoplastic foam shows stress relaxation properties, and the permanent deformation after each cycle is also significant. Based on these results, two main constitutive modeling approaches can be applied for the prediction and the finite element (FE) simulation of structures with varying layers of 3D printed foams. In the elastic regime, a combined viscoelastic and hyperelastic constitutive model should be applied (e.g., the combination of the generalized Maxwell approach with the Ogden's Hyperfoam model) to characterize the nonlinearities and the viscoelastic properties of the foam. On the other hand, when the constitutive modeling also aims to model the permanent deformations, a combined finite strain viscoelastic-viscoplastic material model should be adopted (e.g., the two-layer viscoplastic model – TLVP). This model comprises a Maxwell-type branch in parallel with an elastic-plastic model using isotropic hardening and associative flow rule with Mises yield function, while the

nonlinear viscoelastic effect is modeled using strain- and time-hardening power-law creep models.

Flexural tests

The flexural strength of the different layered samples is shown in Figure 9.

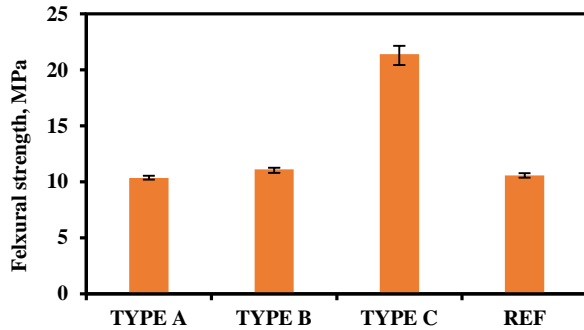


Figure 9. Flexural strength of the multilayer structures

It can be observed that sandwich structures with a decreasing density from top to bottom and the opposite layering with increasing density from top to bottom showed similar results to the reference during bending. In contrast, the Type C sample, which was also produced in a single production step with a rigid shell layer and a foamed core layer, showed more than twice as high flexural strength.

The results show that the one-step production of a solid shell and a foamed core by extrusion-based additive manufacturing technology can also effectively increase the mechanical load resistance (in this case, the flexural stiffness) of the material, which offers the possibility to produce value-added products or to reduce the weight of products while maintaining same mechanical properties.

Conclusions

In this study, the application of in-situ foamable filaments in extrusion-based additive manufacturing was tested to evaluate the effect of printing temperature on foam density, cellular properties, and mechanical properties. The experiments demonstrated that proper adjustment of processing parameters is crucial, as high melt strength inhibits cell expansion, leading to denser structures, while low viscosity causes partial cell collapse and results in inhomogeneous cellular structures.

The experimental results also proved the potential of using extrusion-based additive manufacturing to create density-graded structures with superior mechanical properties, such as increased flexural strength. Based on the material characterization, it can be concluded that due to the highly nonlinear stress-strain curves and the additional inelastic effects, a finite strain viscoelastic-viscoplastic constitutive model should be adopted for the accurate

prediction of 3D-printed foam structures with layers of varying density.

The ability to predict and design such multilayer structures allows for the creation of tailored porosity products that provide optimal functionality. This capability could be exploited in many industrial application fields, such as tailored porosity bone tissue applications in medicine and energy-absorbing structures in the automotive, sports equipment, and packaging sectors. Future work should focus on further refining the finite strain viscoelastic-viscoplastic constitutive model to improve predictive accuracy.

References

1. S.C. Altıparmak, V.A. Yardley, Z. Shi, and J. Lin, *Journal of Manufacturing Processes*, **83**, 607-636 (2022).
2. S.K. Awasthi, M. Kumar, V. Kumar, S. Sarsaiya, P. Anerao, P. Ghosh, L. Singh, H. Liu, Z. Zhang, and M.K. Awasthi, *Environmental Pollution*, **307**, 119600 (2022).
3. K. Litauszki, D. Gere, T. Czigany, and Á. Kmetty, *Sustainable Materials and Technologies*, **35**, e00527 (2023).
4. M. Tomin, and Á. Kmetty, *Journal of Applied Polymer Science*, **139**, 51714 (2022).
5. E. Di Maio, S. Iannace, and G. Mensitieri, Chapter 1 - Foams and their applications, in: E. Di Maio, S. Iannace, G. Mensitieri (Eds.) *Supercritical Fluid Science and Technology*, Elsevier, pp. 1-20, (2021).
6. S. Costeux, *Journal of Applied Polymer Science*, **131**, 41293 (2014).
7. M. Tomin, D. Török, T. Pászthy, and Á. Kmetty, *Polymer Testing*, 108014 (2023).
8. N. Gupta, *Materials Letters*, **61**, 979-982 (2007).
9. Y. Shimazaki, S. Nozu, and T. Inoue, *Polymer Testing*, **54**, 98-103 (2016).
10. K. Kalia, and A. Ameli, *Additive Manufacturing*, **79**, 103945 (2024).
11. P. Song, C. Zhou, H. Fan, B. Zhang, X. Pei, Y. Fan, Q. Jiang, R. Bao, Q. Yang, Z. Dong, and X. Zhang, *Composites Part B: Engineering*, **152**, 151-159 (2018).
12. W.J. Choi, K.S. Hwang, H.J. Kwon, C. Lee, C.H. Kim, T.H. Kim, S.W. Heo, J.-H. Kim, and J.-Y. Lee, *Materials Science and Engineering: C*, **110**, 110693 (2020).
13. A.R. Damanpack, A. Sousa, and M. Bodaghi, *Micromachines*, **12**, 866 (2021).
14. K. Kalia, B. Francoeur, A. Amirkhizi, and A. Ameli, *ACS Applied Materials & Interfaces*, **14**, 22454-22465 (2022).
15. H. Andersson, J. Örtengren, R. Zhang, M. Grauers, and H. Olin, *Additive Manufacturing*, **40**, 101925 (2021).

16. M.E. Curd, N.F. Morrison, M.J.A. Smith, P. Gajjar, Z. Yousaf, and W.J. Parnell, *Composites Part B: Engineering*, **223**, 108952 (2021).
17. Z. Yousaf, M. Smith, P. Potluri, and W. Parnell, *Composites Part B: Engineering*, **186**, 107764 (2020).
18. Y. Kwon, S.E. Seo, J. Lee, S. Berezvai, J. Read de Alaniz, C.D. Eisenbach, R.M. McMeeking, C.J. Hawker, and M.T. Valentine, *Composites Communications*, **37**, 101453 (2023).
19. M. Tomin, and Á. Kmetty, *Journal of Applied Polymer Science*, **138**, 49999 (2021).
20. S. Berezvai, and A. Kossa, *Polymer Testing*, **84**, 106395 (2020).

Acknowledgments

This research was supported by the European Union project: MSCA RISE 872152 - GREEN-MAP - Novel Green Polymeric Materials for Medical Packaging and Disposables to Improve Hospital Sustainability; and by the Hungarian National Research, Development and Innovation Office (K 146236). Szabolcs Berezvai is supported by the Janos Bolyai Research Scholarship of the Hungarian Academy of Sciences.